Current Biology *16*, 825–831, April 18, 2006 DOI 10.1016/j.cub.2006.03.059

Report

Long-Range Directional Movement of an Interphase Chromosome Site

Chien-Hui Chuang,[1] Anne E. Carpenter,[1,3] Beata Fuchsova,[2] Terezina Johnson,[2] Primal de Lanerolle,[2] and Andrew S. Belmont[1,*]
[1] Department of Cell and Developmental Biology
University of Illinois, Urbana-Champaign
Urbana, Illinois 61801
[2] Department of Physiology and Biophysics
University of Illinois at Chicago
Chicago, Illinois 60612

Summary

Increasing evidence suggests functional compartmentalization of interphase nuclei [1]. This includes preferential interior localization of gene-rich and early replicating chromosome regions versus peripheral localization of gene-poor and late replicating chromosome regions [2, 3], association of some active genes with nuclear speckles [4, 5] or transcription "factories" [6], and association of transcriptionally repressed genes with heterochromatic regions [7]. Dynamic changes in chromosome compartmentalization [7–9] imply mechanisms for long-range interphase chromatin movements. However, live cell imaging in mammalian cells has revealed limited chromatin mobility [10], described as "constrained diffusion" [11]. None of these studies, though, have examined a chromosome locus undergoing an inducible repositioning between two different nuclear compartments. Here we demonstrate migration of an interphase chromosome site from the nuclear periphery to the interior 1–2 hr after targeting a transcriptional activator to this site. Spot redistribution is perturbed by specific actin or nuclear myosin I mutants. Extended periods of chromosome immobility are interspersed with several minute periods in which chromosomes move unidirectionally along curvilinear paths oriented roughly perpendicular to the nuclear envelope at velocities of 0.1–0.9 μm/min over distances of 1–5 μm. Our results suggest an active mechanism for fast and directed long-range interphase chromosome movements dependent directly or indirectly on actin/myosin.

Results and Discussion

Previously, we described a simplified system in which tethering the transcription acidic activation domain (AAD) of the viral protein VP16 to a peripheral chromosomal site in CHO DG44 C6 cells led to its repositioning toward the nuclear interior [12]. To visualize the dynamics of this repositioning, we created an inducible VP16 AAD targeting system by using rapamycin-induced heterodimerization of the protein FKBP12 to the protein domain FRB* from the protein FRAP [13, 14] (Figure 1A). The C6 cell line contains a 10–20 copy transgene insertion of a plasmid containing a 256 copy lac operator direct repeat and a DHFR cDNA selectable marker [12]. In C6C8C12 cells, a C6 cell line derivative stably expressing EGFP-lac repressor- $(FKBP12)_3$ and FRB*-VP16 AAD, rapamycin addition induces heterodimerization within the first several minutes, reaching steady state by 15 min [15]. Northern blot analysis reveals increased DHFR transgene transcripts within 60 min, with stable transcript levels reached ~90 min after adding rapamycin (data not shown).

The C6 vector integration site shows a highly preferential localization close to the nuclear periphery. Targeting VP16 AAD in log phase cells resulted in a maximum change in intranuclear distribution 1–2 hr after rapamycin addition, with a slight but characteristic rebound toward steady-state levels by 3 hr (Figure 1B). The observed movement of spots toward the nuclear interior is significant at greater than a 99% confidence level based on a 0.03–0.04 estimated standard deviation of the mean proportion of peripherally associated spots. A nearly identical time course for spot repositioning was obtained for cells blocked in late G1/early S phase by hydroxyurea (HU) (Figure 1C), suggesting similar and efficient chromosome repositioning throughout a large fraction of the cell cycle.

Previously, we showed that targeting VP16 AAD to a gene-amplified, heterochromatic chromosome region resulted in dramatic decondensation of large-scale chromatin structure [16]. More recently, we showed that most acidic activators tested, including activation domains from Gal4, p53, and p65, a component of NF-KB, induced comparable chromatin unfolding [15]. Similarly, the capability of inducing spot redistribution is likely to be a general property of acidic activators, as targeting the mammalian p65 activation domain induced comparable spot migration to the nuclear interior, with nearly identical kinetics, as that seen with the viral VP16 AAD (Figure 1D and data not shown).

Targeting a synthetic acidic peptide, which decondenses large-scale chromatin structure similarly to VP16 but does not activate transcription [15], also induced spot repositioning (Figure 1E). Moreover, inhibiting transcription with DRB had no effect on chromosome repositioning (Figure 1F), while chromosome repositioning after inhibiting transcription with α-amanitin was delayed by ~1 hr (data not shown). We conclude that transcription is not required for long-range movement.

Initial live cell imaging revealed a surprisingly strong photosensitivity of long-range motion to near UV and blue light (Figure 1G, see Figure S1 in the Supplemental Data available with this article online). Control experiments enabled us to identify illumination conditions that produced spot redistribution statistics similar to that observed in cells never exposed to light (Figure 1H, Supplemental Data).

*Correspondence: asbel@uiuc.edu
[3] Present address: Whitehead Institute for Biomedical Research, 9 Cambridge Center, Cambridge, Massachusetts 02142.

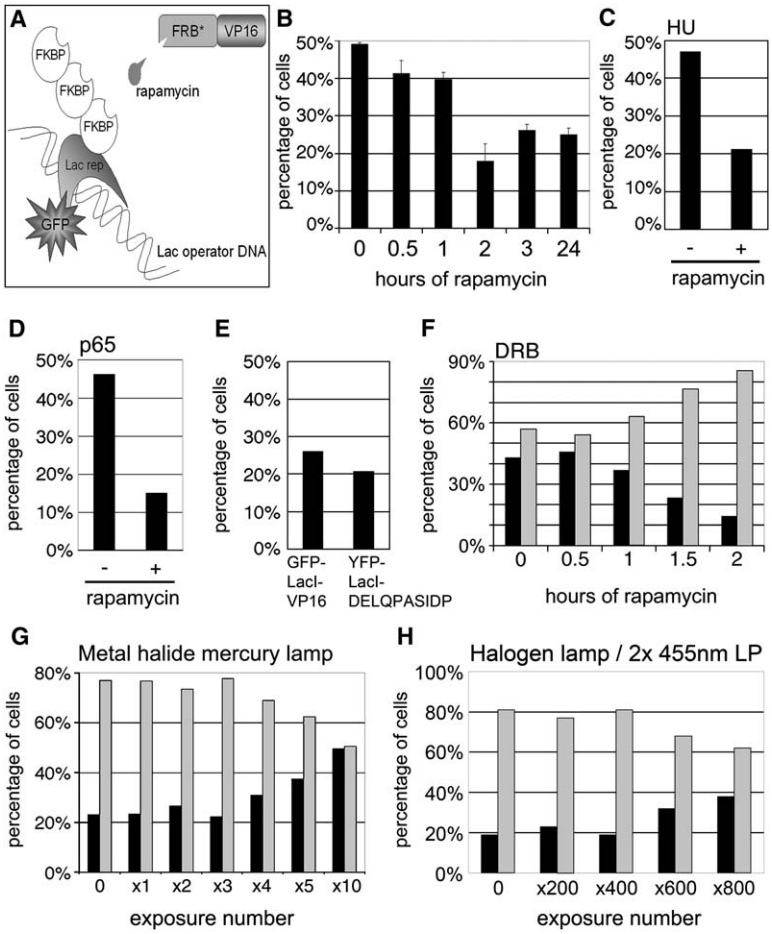

Figure 1. VP16 Induces Chromosome Repositioning from Nuclear Periphery to Interior

(A) EGFP-lac repressor protein with three copies of FKBP12 binds nonfluorescent FRB*-VP16 after rapamycin addition.

(B) Percentage of log phase cells with tagged chromosome spot less than 0.5 μm from nuclear periphery at different times after rapamycin addition (bars represent standard deviation of the mean based on three experiments).

(C–H) Percentage of peripheral (black) versus interior (gray) sites.

(C) Similar redistribution of chromosome site 2 hr after VP16 targeting in cells blocked in late G1/early S.

(D) The acidic activation domain from p65, an endogenous protein, produces similar spot redistribution as seen for the VP16 AAD after targeting induced by rapamycin addition.

(E) Redistribution toward cell interior occurs after targeting an acidic peptide capable of decondensing large-scale chromatin structure but with no transcriptional activity.

(F) Redistribution of chromosome site after transcription inhibition by DRB.

(G and H) Spot redistribution 2 hr after adding rapamycin is dependent on illumination conditions. Data points are from 100–200 cells (C–H) or 300 cells (B).

Under these conditions, live cell imaging confirmed significant long-range chromosome movement induced by VP16 targeting (Figure 2A). Changes in spot distance from the nuclear periphery up to ~2.5 μm in magnitude were observed between 0 and 2 hr after VP16 targeting (Figure 2B, black diamonds), with an average displacement of 1.1 μm and a pronounced bias for movement of spots near the periphery (≤1.5 μm) toward the nuclear interior (positive y values, Figure 2B). Significantly, chromosome displacements between 0 and 2 hr in nearly all cells with targeted VP16 exceeded the largest displacements observed in all three controls (Figure 2B, Figure S2). These controls included the parental C6C8 cells, stably expressing EGFP-lac repressor- $(FKBP12)_3$ but not FRB*-VP16 AAD, to which rapamycin was added (Figure 2B, open circles). Therefore, the observed changes in spot position cannot be attributed to general changes in nuclear and/or chromatin structure induced by rapamycin. They also included C6C8C12 cells to which no rapamycin was added (Figure S2B) and 610 cells containing an interior located spot of comparable size to that in C6 cells (Figure S2C).

Our next goal was to observe the general pattern of movement after VP16 targeting. We divided the 400 minimal exposures permissible without incurring phototoxicity (Figure 1H) by taking 3D data (20 optical sections, 0.075 μm focus step) every 6 min between 0 and 2 hr, during which time 12/15 rapamycin-treated cells, versus 0/15 control cells, showed a spot movement exceeding 1 μm. These data revealed long periods of localized movements punctuated by shorter periods of abrupt, long-range movements, often occurring within only 1–2 6 min intervals (Figure S3 and Supplemental Data). Plotting the mean distance change between adjacent time points as a function of time suggested a mobility peak at ~1 hr after rapamycin addition (data not shown), in agreement with the maximum observed drop in peripheral spot percentage between 1 and 1.5 hr, as measured in fixed cells (data not shown). However, in individual cells, long-range motions could occur before or after this 1 hr time point.

To determine the actual spot trajectories during these short periods of rapid motion, we next collected 3D data (20 optical sections, 0.075 μm focus step) every minute for 20 min. To maximize the percentage of cells observed undergoing long-range motion, we therefore began observations during this period of peak mobility starting 1 hr after adding rapamycin. Approximately 1/3 of cells (14/43) during these 20 min showed long-range chromosome spot movements exceeding 1 μm (Figures 2C–2E), as determined by plots of radial spot distance from the nuclear periphery versus time. (Predictably, this is a lower percentage than observed over the entire 2 hr time period via 6 min data sampling.) To better visualize spot trajectories, we created video images by assembling the most in-focus optical section per time point. Focal changes were minimal during these rapid, long-range movements (Figures 2C–2E).

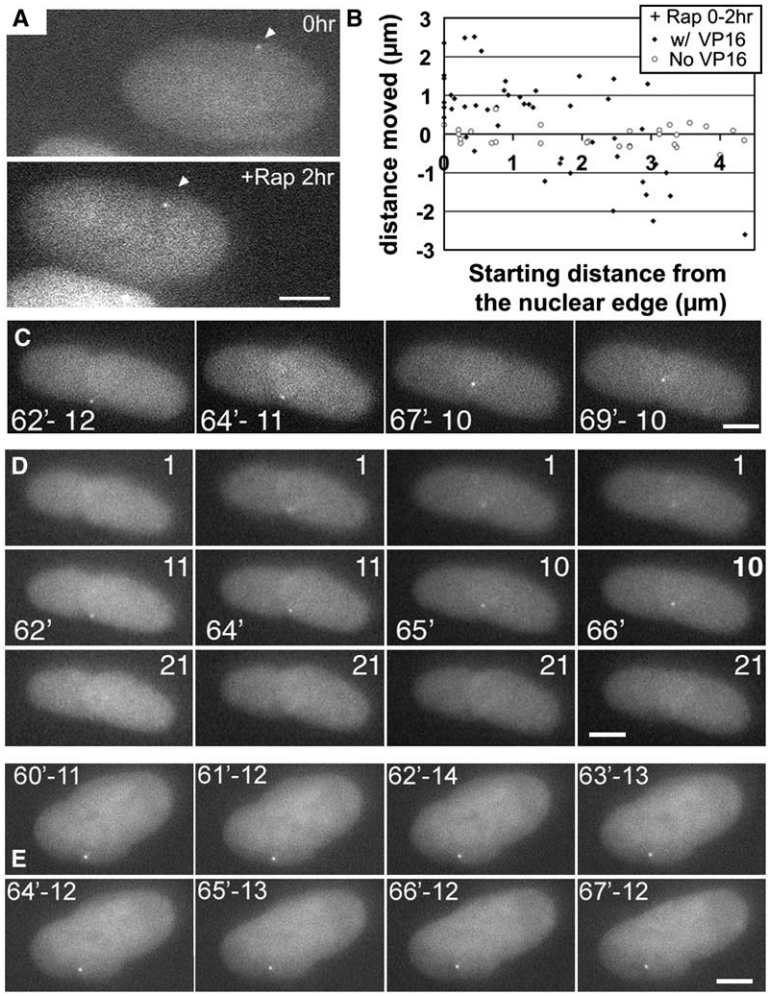

Figure 2. Live Cell Imaging Reveals Long-Range Spot Movements

(A) Chromosome site (arrowheads) has moved toward nuclear interior 2 hr after rapamycin addition.

(B) Scatter plot showing net radial movement of spots between 0 and 2 hr after rapamycin addition in cells expressing FRB*-VP16 (black diamonds) or control cells not expressing FRB*-VP16 (open circles). x axis is starting distance from nuclear periphery, y axis is net radial distance moved toward (positive) or away (negative) from nuclear interior.

(C) Spot undergoing long-range motion: numbers show time in minutes after rapamycin addition followed by optical section number (out of 21) from z-stack (0.075 μm focus step). Movement occurs roughly perpendicular to nuclear envelope. See also Movie S1.

(D) Spot movement occurs without significant change in focus or nuclear shape during period of rapid motion. Optical sections ~0.75 μm below (top) or above (bottom) spot focus (middle) are shown from this period of rapid spot movement. (Upper right, optical section number, 0.075 μm focus step; middle row, panel lower left, time in minutes after rapamycin addition.) See also Movies S1 and S3.

(E) Second example showing spot movement, with minimal changes in focus, from periphery toward the nuclear interior. Numbers shown are as in (C). Scale bars equal 5 μm.

Strikingly, nearly all (12/14) of these video images appeared to show the spots following curvilinear trajectories (Movies S1–S6). The two exceptions were inconclusive due to significant nuclear shape changes during the motion.

To objectively analyze spot trajectories and minimize effects from changes in nuclear position, rotation, or size, a single, in-focus image from each time point was aligned in 2D by a crosscorrelation approach with the image from the preceding time point. Individual 2D images from different time points were projected into a single 2D image to show the 2D spot trajectory (Figure 3). These projected trajectories confirmed a striking linearity to the VP16-induced rapid movements in all cases (10/10) where minimal nuclear shape changes allowed reasonable alignment (Figures 3D–3M). Trajectory lengths varied from 1.3 to 5.2 μm (mean 2.6 μm).

Equally striking was the pronounced trajectory radial bias. 5/10 trajectories were oriented 90° ± 10° with respect to the nuclear periphery, and 9/10 were oriented 90° ± 45°. Assuming random angular distribution between 0° and 180°, the binomial distribution probabilities for ≥5/10 and 9/10 trajectories with these orientations is <.003 and .01, respectively. All aligned trajectories (10/10) and 11/12 total trajectories moved initially toward the nuclear interior ($p < .001$ or .005, respectively), with just 1 trajectory oriented toward the periphery.

Nuclear rotation has been observed in neuronal and other cells with round nuclei [17], raising the question of whether the observed curvilinear motion could be explained by a similar nuclear rotation. Previous work combining nuclear pore staining with optical sectioning demonstrated that the movement of the C6 spot in response to a direct lac repressor-VP16 fusion protein was due to true redistribution of peripheral spots to the nuclear interior [12], and this has been confirmed by the FRB-FBP12-inducible VP16 targeting system in C6C8C12 cells (Figure S5). Moreover, examination of the 2D and 3D image data clearly rules out nuclear rotation as a general explanation for the observed trajectories.

First, the majority of projected trajectory examples shown in Figures 3F–3H and 3J–3M have asymmetries in the trajectory and/or nuclear shape (together with the overall flattened, elliptical nuclear profile, which shows no changes during the motion), which are inconsistent with nuclear rigid-body rotations. One might imagine that compression by the cytoskeleton might lead to a simultaneous nuclear rotation and shape deformation to maintain the flattened nuclear profile. However, it is hard to imagine how a nucleus would simultaneously rotate and deform such that no change in nuclear shape was observed for a spot motion that would have to be explained by an off-axis nuclear

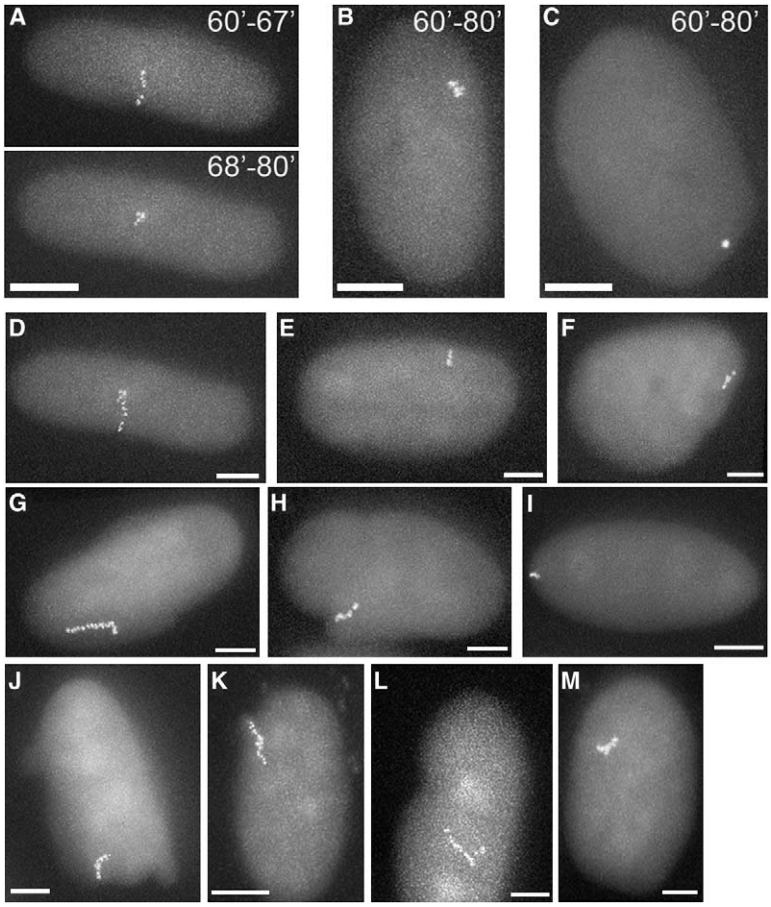

Figure 3. Long-Range, Rapid Movements Show Curvilinear Trajectories

From each time point, the single optical section for which the spot was in focus was extracted from the 3D data stack. A crosscorrelation approach was used to align these 2D images from adjacent time points to correct for nuclear translation and rotation and small changes in nuclear shape, forming an image stack where each section now corresponds to a different time point. This image stack was then projected to yield the spot trajectory over time.

(A) Linear trajectory (60′–67′) is followed by longer period of localized, short-range motion (68′–80′). Time refers to minutes after rapamycin addition. See also Movie S1.

(B and C) Trajectories of a cell not showing long-range motion after rapamycin addition (B) and a control cell (no rapamycin) (C) showing limited, apparently random movements confined within small region. The radius of confinement appears smaller for the control cells versus cells exposed to rapamycin that did not show long-range spot movements (see also Figure 4). See also Movies S5 and S6.

(D–M) Trajectories from cells showing long-range spot movements.

(G) See also Movie S3.

(H) See also Movie S4.

(E) Corresponds to 60′–64′ (see Movie S2), all the rest are 60′–79′. Scale bars equal 5 μm.

rotation. Moreover, spots near the edge of the nucleus still would show significant changes in focus during such combined nuclear rotations and deformations as the conveyer belt-like motion of the nuclear envelope carried the spot from the side of the nucleus to its top or bottom. In fact, measurement of the spot z-position by the optical section stacks from each time point shows variations of only a few tenths of a micron (Figures 2C–2E), relative to an estimated nuclear height of ~3–5 microns, during the period of rapid motion for most of the trajectory examples (5/6 plotted in Figure 4B).

In general, distinguishing nonrandom directed motion from free or constrained diffusion is quite difficult in situations in which both types of motion occur. Even in cases of pure diffusion, a small subset of trajectories will appear linear. However, this is not the case here. Spot trajectories instead appear to fall into two, distinct categories: curvilinear, long-range movements (Figures 3A and 3D–3M) versus constrained motion within a small radius. The latter category was typical of the 29/43 cells in which long-range motion was not observed (Figures 3B and 4C) and all control cells (30), which in general appear to show constrained motion within an even smaller radius (Figures 3C and 4D). Within individual trajectories, short periods of rapid, curvilinear long-range motion (Figure 3A, top) are flanked by constrained motion within a small radius (Figure 3A, bottom). In a few cases, spots follow a linear trajectory, pause for what appears to be small constrained diffusion movements, then resume linear long-range movement at a different angle (Figure S4). During these periods of rapid, directional motion, roughly constant radial velocities (0.14–0.85 μm/min, mean 0.31 μm/min) are observed (Figure 4A). These velocities approach the ~1 μm/min measured for anaphase chromosome movements. No examples of long-range spot movement were observed in 30 control cells not treated with rapamycin, as determined by the plots of radial distance versus time (Figure 4D).

This conclusion of two distinct motion states is supported by a commonly used statistical method for analyzing particle motion by means of the dependence of mean square distance (MSD) with time [18]. Control cells show an initial linearity for spot movements followed by a plateau (Figures 4E and 4F, green), consistent with constrained diffusion models [19]. After VP16 targeting, two cell subpopulations emerge with qualitatively different MSD plots. 29 cells, whose spots do not undergo long-range motion, show a similar constrained diffusion MSD pattern, with increases in diffusion and constraint radii values just a few times larger (Figures 4E and 4F, orange). Differences in MSD plots between these and control cells parallel those previously observed for chromosome regions in mammalian cells associated or not associated with the nuclear periphery or nucleoli [10]. In contrast, cells undergoing long-range motion produce a qualitatively different MSD plot (Figure 4E, red, blue). MSD values are ~50-fold higher than in control cells. Moreover, MSD values continue to increase with

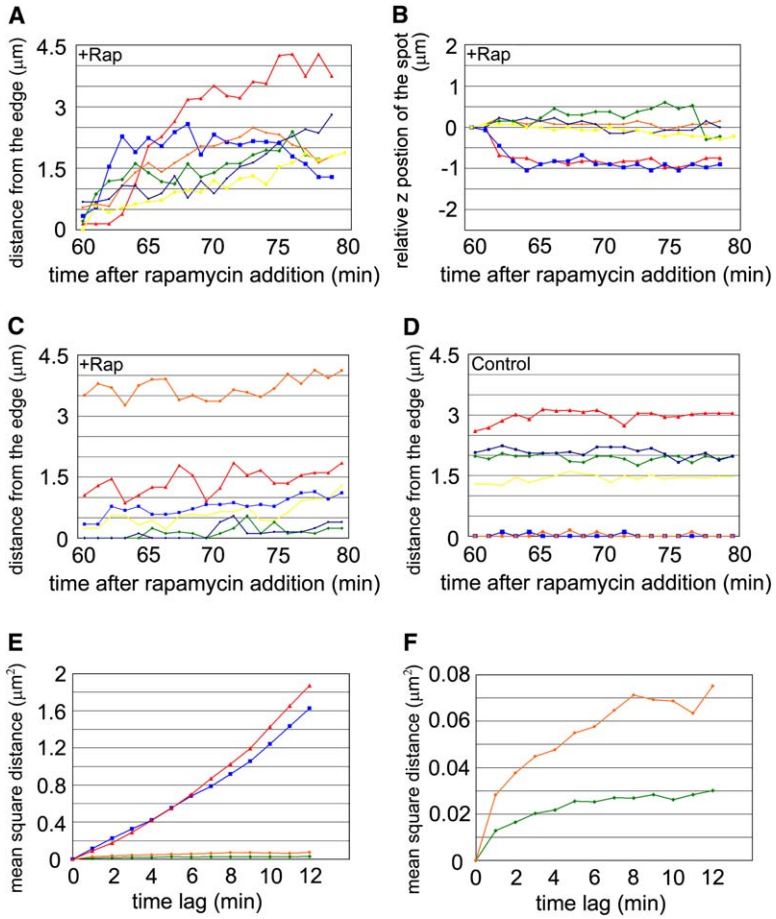

Figure 4. Two Qualitatively Different Mobility Regimes—Rapid, Long-Range Mobility Is Distinct from Short-Range, Localized Mobility

(A) Distance from nuclear periphery versus time—during short periods of rapid, long-range motion, roughly constant velocities (i.e., linear plots) are observed. Red plot corresponds to cell shown in Figures 2C, 2D, 3A, and 3D orange plot corresponds to cell shown in Figures 2E and 3G. See also Movies S1–S4.

(B) Relative changes in focus for same cells shown in (A).

(C) Distance from nuclear periphery versus time for spots from cells treated with rapamycin but not showing long-range movements. Fluctuations in distance from nuclear envelope appear several times larger than observed in control cells (no rapamycin), which show only small position fluctuations and no persistent, unidirectional, long-range movements (D).

(E and F) Mean square distance from periphery versus time lag shows qualitative differences in mobility. (E) Averages from 14 trajectories showing long-range motion (blue), including 10 curvilinear trajectories from aligned data sets (red), versus 29 spot trajectories (orange in [E] and [F]), which did not show long-range motion after rapamycin addition, and 30 control trajectories (green in [E] and [F]).

a noticeable concave shape, consistent with "free diffusion" superimposed on "velocity flow" or directed motion [19].

We next began to address the molecular basis of this spot long-range movement. Actin [20] and an isoform of myosin IC [21] have been identified in the nucleus. Immunofluorescence microscopy demonstrated the recruitment of this nuclear myosin I (NMI) by VP16 to a large, gene-amplified chromosome array (Figure 5A). Colocalization is partial but significant, covering a large extent of the GFP signal. Spot redistribution after VP16 targeting was delayed several hours after transient transfection of a mutant NLS-tagged NMI (E407V) (Figure 5B), with the change in percentage of peripheral spots not becoming statistically significant at greater than the 99% confidence level until 5 hr after rapamycin addition, versus 2 hr for the control. The corresponding mutation (E470A) in the smooth muscle myosin II heavy chain locks myosin II into a weak actin binding state, blocking in vitro actin filament motility [22]. Normal spot redistribution was observed after transfection with the NLS-tagged myopathy loop deletion NMI mutant (Figure 5C). The myopathy loop is in a putative actin binding site; myopathy loop deletions in myosin II still exhibit motor activities, although at lower levels [23].

Spot redistribution was blocked by BDM (2-3-Butanedione monoxime) (Figure 5D). Although BDM has been widely used as a nonmuscle myosin inhibitor, recent work has shown no inhibition for several nonmuscle myosins but rather inhibition of actin dynamics [24]. Transient expression of mRFP-actin-NLS had no effect on spot redistribution kinetics (Figure 5F, gray bars). Transfected cells were identified based on their nuclear mRFP fluorescence, with nontransfected cells on the same coverslips serving as controls. However, expression of a similarly tagged, nonpolymerizable mutant actin (G13R) [25] completely blocked spot redistribution after VP16 targeting (Figure 5E). In distinct contrast, a tagged, mutant actin (S14C), which stabilizes F-actin [26], instead shifted the spot redistribution toward earlier times (Figure 5F). The characteristic minimum in peripherally located spots shifted from 2 to 1.5 hr after rapamycin addition, with the percentage of peripheral spots first becoming statistically significantly lower at greater than the 99% confidence level at 1 hr after rapamycin addition versus 1.5 hr for the wild-type actin control. Moreover, the percentage of peripheral spots for the wild-type actin control versus the S14C mutant at 1 hr after rapamycin addition are different at a 99% confidence level, while the wild-type value at 1.5 hr after rapamycin addition is identical to the S14C value at 1 hr after rapamcyin addition at greater than a 99% confidence level. From this we conclude that expression and nuclear targeting of the F-actin stabilizing actin construct causes an acceleration of ~0.5 hr in the rapamycin-induced spot redistribution to the nuclear interior.

Our results reveal for the first time an active and physiologically regulated translocation mechanism for

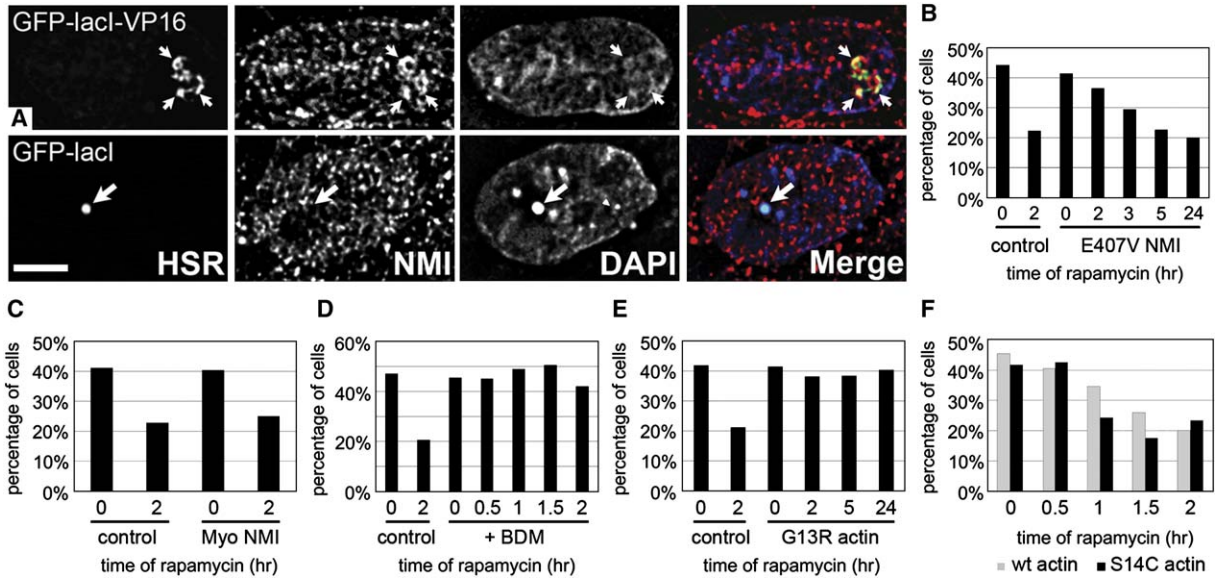

Figure 5. Functional Analysis of Actin and Myosin in Spot Migration

(A) Recruitment of nuclear myosin I (red) to A03 amplified chromosome region (homogeneous staining region, HSR) containing lac operator sites (arrows) after expression of EGFP-lac repressor-VP16 AAD (green). No recruitment was seen after expression of EGFP-lac repressor (green). Scale bar equals 5 μm.

(B–F) Percentage of cells with peripheral chromosome location (averages from two [B–E] or three [F] experiments, 100 cells each).

(B) 3 hr delay in spot redistribution in cells expressing E407 NMI relative to control, nontransfected cells.

(C) No delay in cells expressing NMI with myopathy loop deletion.

(D) BDM blocks spot redistribution.

(E) Expression of mRFP-NLS-G13R mutant actin defective in polymerization blocks spot movement at all times.

(F) S14C actin mutant, favoring F-actin polymerization, accelerates spot redistribution (black) relative to wild-type actin (gray).

long-range, directed interphase chromosome movements. We suggest previous failures to observe long-range interphase chromosome movements in mammalian cells by live cell imaging were likely due to two reasons. First, the default for interphase chromatin in mammalian cells appears to be constrained diffusion with chromatin mobility confined to small regions [10, 11]. This implies that long-range chromatin movements are under tight physiological regulatory control, with only specific chromosome regions undergoing long-range motion, and only under special circumstances and for short time periods. Second, this motion appears to be unusually photosensitive and blocked by even short exposures with conventional microscope configurations.

Our findings provoke a number of fundamental, cell biological questions. What are the molecular mechanism and possible motors for directed interphase chromosome movements? We demonstrated long-range chromatin movement dependent on actin and nuclear myosin. The exact molecular mechanism underlying this dependence—whether it is direct or indirect—remains unknown. However, the elimination of spot redistribution by an actin point mutation defective in actin polymerization and the accelerated spot redistribution with an actin mutant that favors F-actin formation raises the tantalizing possibility that the mechanism for long-range chromatin movement directly involves F-actin and myosin. Previously, we demonstrated that the lac operator-tagged spot in C6 cells also shows a cell cycle-dependent motion during early S phase into the nuclear interior in the absence of any targeted transcription factor [12]. Experiments now in progress (C.-H.C. and A.S.B., unpublished data) indicate that this cell cycle-related motion is also blocked by BDM addition, suggesting that long-range chromosome movements dependent on actin/myosin may be a more general phenomenon not restricted to our current transcription factor-induced model for chromosome movement.

We can envision two alternative scenarios for such a direct, active involvement. First, actin/myosin could be required to actively target the spot to the nuclear periphery, requiring stretching of the flanking interphase chromosome regions anchored distally to interior structures. Release of the spot attachment to the nuclear periphery would then lead to an elastic "recoil" with rapid motion into the interior. We consider this model unlikely. It does not explain examples in which the spot moves in one direction, stops, then moves at a different angle. It appears inconsistent with the observed near constant velocity during periods of rapid motion. It is also inconsistent with our data showing a higher local mobility of the spot after VP16 targeting, in cells in which long-range motion is not occurring, as if the spot is no longer firmly anchored to the nuclear periphery. Finally, this model predicts that the percentage of spots localized to the periphery in the absence of rapamycin might be expected to decrease after expression of actin and myosin mutants. The alternative scenario is that the inward spot movement after transcription factor targeting directly involves actin/myosin.

Independent of the mechanism for active movement per se, additional questions include what provides directionality to this movement? What establishes the apparent radial polarity within the nucleus? What is the

relationship between changes in nuclear position and transcriptional and/or epigenetic reprogamming?

Future work will exploit our simplified, engineered system to begin to address these questions.

Supplemental Data

Supplemental Data include five figures, six movies, and Supplemental Experimental Procedures and can be found with this article online at http://www.current-biology.com/cgi/content/full/16/8/825/DC1/.

Acknowledgments

This work was supported by NIH grants GM42516 and GM58460 to A.S.B. and in part by NIH grant GM56489 and NSF grants INT 9724168 and ID 0517468 to P. de L. A.E.C. was supported by a Howard Hughes Medical Institute predoctoral fellowship. We thank Roger Tsien (UCSD) for supplying mRFP1-pRSETB and Tudorita Tumbar (Cornell University) and Volodya Gelfand (Northwestern Medical School) for their critical reading of this manuscript.

Received: October 11, 2005
Revised: March 6, 2006
Accepted: March 7, 2006
Published: April 17, 2006

References

1. Spector, D.L. (2003). The dynamics of chromosome organization and gene regulation. Annu. Rev. Biochem. *72*, 573–608.
2. Croft, J.A., Bridger, J.M., Boyle, S., Perry, P., Teague, P., and Bickmore, W.A. (1999). Differences in the localization and morphology of chromosomes in the human nucleus. J. Cell Biol. *145*, 1119–1131.
3. Ferreira, J., Paolella, G., Ramos, C., and Lamond, A.I. (1997). Spatial organization of large-scale chromatin domains in the nucleus: a magnified view of single chromosome territories. J. Cell Biol. *139*, 1597–1610.
4. Smith, K.P., Moen, P.T., Wydner, K.L., Coleman, J.R., and Lawrence, J.B. (1999). Processing of endogenous pre-mRNAs in association with SC-35 domains is gene specific. J. Cell Biol. *144*, 617–629.
5. Carter, K.C., Bowman, D., Carrington, W., Fogarty, K., McNeil, J.A., Fay, F.S., and Lawrence, J.B. (1993). A three-dimensional view of precursor messenger RNA metabolism within the mammalian nucleus. Science *259*, 1330–1335.
6. Osborne, C.S., Chakalova, L., Brown, K.E., Carter, D., Horton, A., Debrand, E., Goyenechea, B., Mitchell, J.A., Lopes, S., Reik, W., et al. (2004). Active genes dynamically colocalize to shared sites of ongoing transcription. Nat. Genet. *36*, 1065–1071.
7. Fisher, A.G., and Merkenschlager, M. (2002). Gene silencing, cell fate and nuclear organisation. Curr. Opin. Genet. Dev. *12*, 193–197.
8. Parada, L., and Misteli, T. (2002). Chromosome positioning in the interphase nucleus. Trends Cell Biol. *12*, 425–432.
9. Francastel, C., Schubeler, D., Martin, D.I., and Groudine, M. (2000). Nuclear compartmentalization and gene activity. Nat. Rev. Mol. Cell Biol. *1*, 137–143.
10. Chubb, J.R., Boyle, S., Perry, P., and Bickmore, W.A. (2002). Chromatin motion is constrained by association with nuclear compartments in human cells. Curr. Biol. *12*, 439–445.
11. Marshall, W.F., Straight, A., Marko, J.F., Swedlow, J., Dernburg, A., Belmont, A., Murray, A.W., Agard, D.A., and Sedat, J.W. (1997). Interphase chromosomes undergo constrained diffusional motion in living cells. Curr. Biol. *7*, 930–939.
12. Tumbar, T., and Belmont, A.S. (2001). Interphase movements of a DNA chromosome region modulated by VP16 transcriptional activator. Nat. Cell Biol. *3*, 134–139.
13. Choi, J., Chen, J., Schreiber, S.L., and Clardy, J. (1996). Structure of the FKBP12-rapamycin complex interacting with the binding domain of human FRAP. Science *273*, 239–242.
14. Liberles, S.D., Diver, S.T., Austin, D.J., and Schreiber, S.L. (1997). Inducible gene expression and protein translocation using nontoxic ligands identified by a mammalian three-hybrid screen. Proc. Natl. Acad. Sci. USA *94*, 7825–7830.
15. Carpenter, A.E., Memedula, S., Plutz, M.J., and Belmont, A.S. (2005). Common effects of acidic activators on large-scale chromatin structure and transcription. Mol. Cell. Biol. *25*, 958–968.
16. Tumbar, T., Sudlow, G., and Belmont, A.S. (1999). Large-scale chromatin unfolding and remodeling induced by VP16 acidic activation domain. J. Cell Biol. *145*, 1341–1354.
17. De Boni, U., and Mintz, A.H. (1986). Curvilinear, three-dimensional motion of chromatin domains and nucleoli in neuronal interphase nuclei. Science *234*, 863–866.
18. Carmo-Fonseca, M., Platani, M., and Swedlow, J.R. (2002). Macromolecular mobility inside the cell nucleus. Trends Cell Biol. *12*, 491–495.
19. Saxton, M.J. (1994). Single-particle tracking: models of directed transport. Biophys. J. *67*, 2110–2119.
20. Bettinger, B.T., Gilbert, D.M., and Amberg, D.C. (2004). Actin up in the nucleus. Nat. Rev. Mol. Cell Biol. *5*, 410–415.
21. Pestic-Dragovich, L., Stojiljkovic, L., Philimonenko, A.A., Nowak, G., Ke, Y., Settlage, R.E., Shabanowitz, J., Hunt, D.F., Hozak, P., and de Lanerolle, P. (2000). A myosin I isoform in the nucleus. Science *290*, 337–341.
22. Kad, N.M., Rovner, A.S., Fagnant, P.M., Joel, P.B., Kennedy, G.G., Patlak, J.B., Warshaw, D.M., and Trybus, K.M. (2003). A mutant heterodimeric myosin with one inactive head generates maximal displacement. J. Cell Biol. *162*, 481–488.
23. Sasaki, N., Asukagawa, H., Yasuda, R., Hiratsuka, T., and Sutoh, K. (1999). Deletion of the myopathy loop of Dictyostelium myosin II and its impact on motor functions. J. Biol. Chem. *274*, 37840–37844.
24. Yarrow, J.C., Lechler, T., Li, R., and Mitchison, T.J. (2003). Rapid de-localization of actin leading edge components with BDM treatment. BMC Cell Biol. *4*, 5.
25. Posern, G., Sotiropoulos, A., and Treisman, R. (2002). Mutant actins demonstrate a role for unpolymerized actin in control of transcription by serum response factor. Mol. Biol. Cell *13*, 4167–4178.
26. Posern, G., Miralles, F., Guettler, S., and Treisman, R. (2004). Mutant actins that stabilise F-actin use distinct mechanisms to activate the SRF coactivator MAL. EMBO J. *23*, 3973–3983.